NOVEL NANOMETRIC SUPERSTRUCTURES FOR RADIATION AND MAGNETIC SENSING

Jimmy Xu

Brown University, Box D
184 Hope Street
Providence, RI 02912

22 May 2007

Final Report

APPROVED FOR PUBLIC RELEASE; DISTRIBUTION IS UNLIMITED.

AIR FORCE RESEARCH LABORATORY
Space Vehicles Directorate
3550 Aberdeen Ave SE
AIR FORCE MATERIEL COMMAND
KIRTLAND AIR FORCE BASE, NM 87117-5776

NOTICE AND SIGNATURE PAGE

Using Government drawings, specifications, or other data included in this document for any purpose other than Government procurement does not in any way obligate the U.S. Government. The fact that the Government formulated or supplied the drawings, specifications, or other data does not license the holder or any other person or corporation; or convey any rights or permission to manufacture, use, or sell any patented invention that may relate to them.

This report was cleared for public release by the Air Force Research Laboratory/PRS Public Affairs Office and is available to the general public, including foreign nationals. Copies may be obtained from the Defense Technical Information Center (DTIC) (http://www.dtic.mil).

AFRL-VS-PS-TR-2007-1091 HAS BEEN REVIEWED AND IS APPROVED FOR PUBLICATION IN ACCORDANCE WITH ASSIGNED DISTRIBUTION STATEMENT.

//signed//	//signed//
DANHONG HUANG Program Manager	JOHN P. BEAUCHEMIN, Lt Col, USAF Deputy Chief, Spacecraft Technology Division Space Vehicles Directorate

This report is published in the interest of scientific and technical information exchange, and its publication does not constitute the Government's approval or disapproval of its ideas or findings.

REPORT DOCUMENTATION PAGE

Form Approved
OMB No. 0704-0188

Public reporting burden for this collection of information is estimated to average 1 hour per response, including the time for reviewing instructions, searching existing data sources, gathering and maintaining the data needed, and completing and reviewing this collection of information. Send comments regarding this burden estimate or any other aspect of this collection of information, including suggestions for reducing this burden to Department of Defense, Washington Headquarters Services, Directorate for Information Operations and Reports (0704-0188), 1215 Jefferson Davis Highway, Suite 1204, Arlington, VA 22202-4302. Respondents should be aware that notwithstanding any other provision of law, no person shall be subject to any penalty for failing to comply with a collection of information if it does not display a currently valid OMB control number. **PLEASE DO NOT RETURN YOUR FORM TO THE ABOVE ADDRESS.**

1. REPORT DATE *(DD-MM-YYYY)*	2. REPORT TYPE	3. DATES COVERED *(From - To)*
22/05/2007	Final Report	22/08/2002 to 00/05/2007

4. TITLE AND SUBTITLE
Novel Nanometric Superstructures for Radiation and Magnetic Sensing

5a. CONTRACT NUMBER
F29601-02-C-0214

5b. GRANT NUMBER

5c. PROGRAM ELEMENT NUMBER
62601F

6. AUTHOR(S)
Jimmy Xu

5d. PROJECT NUMBER
4846

5e. TASK NUMBER
CR

5f. WORK UNIT NUMBER
A1

7. PERFORMING ORGANIZATION NAME(S) AND ADDRESS(ES)

Division of Engineering
Brown University
Box D
Providence, RI 02912

8. PERFORMING ORGANIZATION REPORT NUMBER

9. SPONSORING / MONITORING AGENCY NAME(S) AND ADDRESS(ES)
Air Force Research Laboratory
Space Vehicles Directorate
3550 Aberdeen Ave., SE
Kirtland AFB, NM 87117-5776

10. SPONSOR/MONITOR'S ACRONYM(S)
AFRL/VSSS

11. SPONSOR/MONITOR'S REPORT NUMBER(S)
AFRL-VS-PS-TR-2007-1091

12. DISTRIBUTION / AVAILABILITY STATEMENT
Approved for public release; distribution is unlimited. (Clearance #07.005-197)

13. SUPPLEMENTARY NOTES

14. ABSTRACT

The desired extreme uniformity and dense packing of quantum electric elements over a large area combined with the nanoscale features of the structures (2D or 3D superlattices) have made their fabrications a great challenge for the conventional e-beam lithography based approaches. In the case of applications that require yet larger area than semiconductor wafers and/or conformation to curved surfaces, as often required in radiation sensing, it is even beyond the reach of conventional nanofabrication approaches. The difficulty in fabrication has impeded the development of the sensing devices and slowed down the progress in understanding the underlying physics and potential of nanostructures. To address these needs and challenges, we have pursued successfully the development of alternative nanofabrication approaches, based on non-lithographical patterning. These new nano-fabrication approaches have then be applied to the development of a new class of nanomaterials – lateral nanodot, nanopost, and nanoantidot superlattices – with unprecedented uniformity, scalability, and versability. The suite of novel nanofabrication technologies and the new class of nanomaterials, resulting from this project, have enabled a number of advances in sensing applications and are expected to lead to new applications in remote sensing and other DoD interests.

15. SUBJECT TERMS
Nanofabrication, Sensing, Infrared, Plasmon, Quantum Wire, Quantum Dot

16. SECURITY CLASSIFICATION OF:			17. LIMITATION OF ABSTRACT	18. NUMBER OF PAGES	19a. NAME OF RESPONSIBLE PERSON
a. REPORT	b. ABSTRACT	c. THIS PAGE			Dr. DanHong Huang
Unclassified	Unclassified	Unclassified	Unlimited	30	19b. TELEPHONE NUMBER *(include area code)* (505) 846-5788

Standard Form 298 (Rev. 8-98)
Prescribed by ANSI Std. 239.18

TABLE OF CONTENTS

FIGURES

TABLES

1. **Summary**

1.1. Rationale:

Nanoscaled structures and systems with critical feature sizes much smaller than the wavelength of electromagnetic radiation signals have been studied in detail in this work for their potential applications in remote sensing and space systems. Detailed understanding of the unique properties arising from strong collective electronic and photonic couplings of such nanostructures has been pursued in order to optimize and utilize these effects and to discover new pathways that can lead to new sensing devices and technologies.

1.2 Challenges:

The desired extreme uniformity and dense packing of quantum electronic elements over a large area combined with the nanoscale features of the structures (2D or 3D superlattices), as proposed in this work, have made their fabrication a great challenge for the conventional e-beam lithography-based approaches. In the case of applications that require yet larger area than semiconductor wafers and/or conformation to curved surfaces, as often required in radiation sensing, it is even beyond the reach of conventional nanofabrication approaches. The difficulty in fabrication naturally has impeded the development of the sensing devices and slowed down the progress in understanding the underlying physics and potential of nanostructures.

1.3 Advances and accomplishments on all three fronts:

(a) To address the needs and challenges identified at the inception of the project, as outlined above, we pursued successfully the development of alternative nanofabrication approaches, based on non-lithographical patterning.

(b) These new nano-fabrication approaches have then be applied to the development of a new class of nanomaterials – lateral nanodot, nanopost, and nanoantidot superlattices – with unprecedented uniformity, scalability, and versatility.

(c) The suite of novel nanofabrication technologies and the new class of nanomaterials, resulting from this project, have enabled a number of advances in sensing device applications, have offered long-lasting value to, and are expected to lead to new applications in the field of remote sensing and other DoD interests.

Tangible examples of the accomplishments in each of the above three categories are described in the sections below, many of which have been reported in great detail in refereed journal papers as listed in the publication section.

1.4 Scope

To provide a platform that can enable as wide a range of sensing interests as possible, we set out to tackle a large range of materials and structure features, spanning across several fields – (1) Semiconductor-based nano-dots, nano-pillars, nano-heterojunctions and nano-cavities; (2) Organic-inorganic nanocomposite superlattices; (3) Metallic, magnetic, and metal-oxide nano-dots, nano-wires, and nano-meshes; and (4) Superconducting lateral superlattices.

While a large range of materials and structures is needed for applications, the fabrication technologies are preferably to be kept as simple and material-independent as possible. This project attempted to accomplish both and has produced a rich set of results and technology advances ready for, and being transitioned to, the AFRL and the DoD community at large.

2. METHODS AND APPROACHES

Fabricating nanostructures and tailoring their properties on the length scales smaller than 50 nm are still quite challenging for most methods. And, making them in large highly ordered, densely packed, and uniform arrays, to enable and enhance desirable collective behaviors as needed in remote sensing, is even more difficult [P1, R1, R2], even for the state-of-the-art e-beam lithography technology. Scaling beyond the size of semiconductor wafers and/or conforming to curved surfaces is generally beyond the reach of existing methods. To overcome these difficulties, a non-lithographic nanofabrication method was devised, developed, extended, and optimized over the course of this project. Central to the non-lithographic nanofabrication method is the utilization of an alumina nanopore membrane as either the growth template, or etch or evaporation mask for the formation of the proposed nanostructures. Figure 1 schematically shows the base fabrication process flows developed for fabricating all the lateral superlattices presented in this report.

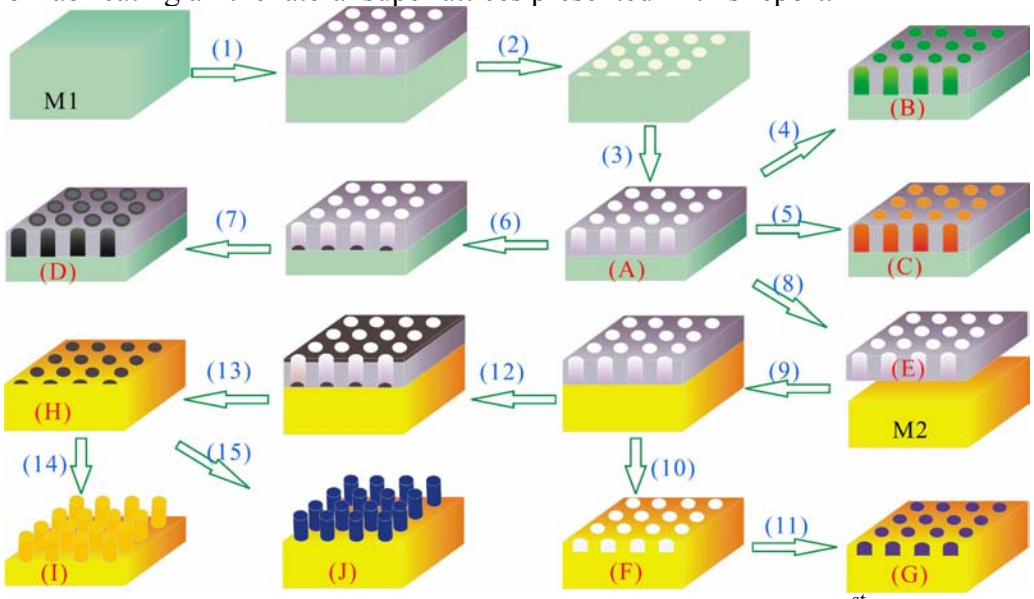

Figure 1. Schematic illustration of nanofabrication processes: (1) 1st anodization; (2) removal of anodized alumina; (3) 2nd anodization; (4) electrodeposition; (5) sol-gel deposition or filling; (6) electrodeposition of catalyst; (7) CVD carbon nanotube growth; (8) removal of aluminum substrate and alumina barrier; (9) transfer of alumina membrane onto other substrate; (10) RIE etching; (11) epitaxial growth; (12) e-beam evaporation; (13) removal of alumina mask; (14) RIE etching; (15) CVD or VLS growth. The nanostructures obtained from the above processes include: (A) alumina template; (B) nanowire array; (C) metal/oxide nanotube or nanowire array; (D) carbon nanotube array; (E) freestanding alumina film/mask; (F) anti-dot array; (G) quantum-dot array; (H) nano-dot array; (I) quantum-wire / nano-pillar array; (J) nanowire or nanotube array. The starting materials are aluminum sheet (M1) and semiconductor substrate (M2).

As shown in the flow chart above, the base process could branch out into several directions – growth, etching, physical filling, and electrodeposition.

2.1. Alumina template and mask fabrication methods

2.1.1. Fabrication of the alumina template on aluminum

To fabricate the alumina nanopore array membrane, an aluminum sheet or foil was anodized in an acid solution (oxalic, sulfuric or phosphoric acid). In the anodization process, an electrical circuit was established between a cathode and the aluminum sheet or foil which served as the anode. Highly ordered hexagonally arranged pore arrays can be obtained under finely controlled conditions. During the anodization, initially a planar barrier layer forms and is followed by pore development leading to the formation of the relatively regular porous anodic film. After an initial period of anodization of tens of minutes, a steady-state pore growth regime is reached that is characterized by the balance between the field-enhanced oxide dissolution at the oxide/electrolyte interface at the pore bottom and the formation of oxide at the metal/oxide interface. The cell and pore diameters, and the thickness of the oxide barrier layer separating the porous alumina and the aluminum, are directly proportional to the anodization voltage.

A two-step anodization process can improve the pore regularity under particular conditions [R3]. In this process, after removing the thick aluminum oxide film obtained from the first long anodization, the aluminum surface is imprinted with a highly ordered dimple array. Then, a porous alumina film with highly ordered pore array, which is a replication to the dimples, can be obtained by a subsequent re-anodization under the appropriate conditions. It should be mentioned here that the two-step approach is necessary, especially in the case of using alumina film as etch or evaporation mask.

2.1.2. Fabrication of alumina mask

To prepare the alumina mask, first, a very thin layer of aluminum oxide, typically with thickness of 300 – 700 nm, was generated during the second anodization. Next, in order to obtain a free standing porous alumina mask, we created a wet-etching process by selectively removing the aluminum substrate and the alumina barrier layer using diluted mercury chloride solution and 0.5 M phosphoric acid, respectively. Then, the alumina film was intensively cleaned with care and transferred onto a substrate by picking up the film floating in the solution by the substrate.

2.1.3. Direct formation of the alumina template on semiconductor substrates

To make an alumina film directly on a semiconductor substrate, an unprecedentedly thick aluminum film was first deposited onto the substrate by e-beam evaporation using a specially designed high vacuum evaporator equipped with a custom-made substrate holder, featuring temperature control and axial rotation to allow in situ annealing with minimal oxidation and high film uniformity. The anodization of the aluminum film followed the same procedures as stated above.

2.2. Nanometric superstructure fabrication methods

In the following, we present a summary of all the methods used in this project for fabrication of the nanometric superstructures:

2.2.1. Chemical vapor deposition (CVD)

CVD is a common method for fabricating carbon nanotubes in large quantities, though there are other processes such as arc-discharge, laser vaporization of graphite targets, and electrolysis of carbon electrodes in molten ionic salts. The CVD process involves the decomposition of hydrocarbons (e.g. methane, acetylene, etc) over metal catalysts (e.g. Co, Ni, Fe, etc). Our group was the first one to produce highly ordered carbon nanotube arrays by applying alumina templates for CVD carbon nanotube growth. Carbon nanotubes with unprecedented uniformity both in diameter and length were obtained [R4].

2.2.2. Vapor-liquid-solid (VLS) growth method

This method was used for growth of metallic oxide nanowires or nanorods in alumina templates or on semiconductor substrates by catalyst particles. We developed a low temperature (~450^{o}C) growth process for ZnO nanowires / nanorods growth using $ZnAs_2$ as precursor and gold nanodots as catalyst [P2].

2.2.3. Electrodeposition

Using alumina film as template, highly ordered metallic or semiconductor nanowire arrays were obtained. We developed and optimized the electrochemical deposition process with controlled growth and high uniformity in nanowire length by introducing an organic solution bath. Highly ordered nanowire arrays of Ni, Co, Fe, and Bi, etc., were readily obtained [R5]. This process was also tailored for catalyst deposition using ac electrical power for templated growth of carbon nanotubes.

2.2.4. Electroless deposition

Electroless deposition was used for fabrication of metallic nanotubes, such as gold and nickel nanotubes, using alumina films as templates. We figured out that the key aspect of this process is the wet ability of the inner wall of the alumina nanochannel. To guarantee deposition uniformity, three measures were taken into action including (1) use of organic solvent, such as methanol, to wet the pore, for methanol has higher permeability/mobility than water; (2) filling pore under vacuum conditions to help eliminate gas/air bubbles inside the pores; and (3) modification of inner wall of the alumina pore using polymers, e.g., polylysine.

2.2.5. Sol-gel method

This method was applied to obtain oxide nanotubes or nanowires (e.g., silica) as well as for modification of the pore size and inner wall properties of the alumina template. The same measures for electroless deposition as stated above were applied to this process, too.

2.2.6. E-beam evaporation

E-beam evaporation was used for fabrication of various nano-dot arrays (e.g., gold, silver, nickel, cobalt, iron, niobium, etc.) using thin alumina film as material evaporation mask. It was used for preparation of high-quality aluminum films with unprecedented

thickness on silicon substrates as well. We also produced very thin nanostructured metallic or oxide films by evaporating metal or oxide onto alumina templates.

2.2.7. Reactive ion etching (RIE)

Through RIE, nano-pillar arrays or anti-dot arrays on semiconductor substrates can be obtained by using the above evaporated nano-dot array as the etching mask or directly using alumina film as the etching mask. RIE also was used for cleaning samples or materials.

2.2.8. Molecular beam epitaxial (MBE) growth

This is for epitaxial growth of quantum-dots into nanocavities by using anti-dot array on semiconductors as growth template.

2.3. Materials characterization methods

We used various means for characterization of morphological, crystallitic, chemical, electronic, magnetic, and optical properties of the nanostructures. The following methods were frequently used:

2.3.1. AFM (Atomic Force Microscope) and MFM (Magnetic Force Microscope)
2.3.2. SEM (Scanning Electron Microscope)
2.3.3. TEM (Transmission Electron Microscope) and HRTEM (High Resolution TEM)
2.3.4. EDX (Energy Dispersive X-ray) and XRD (X-Ray Diffraction)
2.3.5. FTIR (Fourier Transfer Infrared Spectroscopy)
2.3.6. Raman Spectroscopy
2.3.7. PL (Photoluminescence)
2.3.8. Other standard electrical and magnetic measurements

3. RESULTS AND DISCUSSIONS

3.1. Alumina template and mask

The advantage of using alumina template or mask is that the fabrication process is scaleable, controllable, and economical. Moreover, an alumina template can be grown on curved or any arbitrary surfaces, which was detailed in a most recently published paper [P3].

3.1.1. Highly ordered alumina pore array

As stated above, the feature sizes (pore diameters, inter-pore distances) and ordering of pores are highly dependent of the anodization conditions including type, concentration and temperature of electrolyte, anodization voltage, and anodization duration. To obtain highly ordered pore arrays over a large feature size range, we optimized the anodization conditions as shown in Table 1. Figure 2 shows AFM images of the highly ordered pore arrays and a cross-section view SEM image of the uniformity of the ultimately straight pore channels.

Table 1. Optimized anodization conditions for obtaining highly ordered alumina pore arrays with different feature sizes.

		Sulfuric Acid			Oxalic Acid	Phosphoric Acid
Concentration (M)		3.5	1.5	0.5	0.3	0.5-1
Anodization voltage (V)		10	18	25	40	160-196
Temperature (^{o}C)		0-2	0-2	2-10	2-10	0-2
Feature size	Pore diameter (nm)	10-15	18-23	25-30	40-50	200-250
	Inter-pore distance (nm)	25-35	40-50	60-70	~100	400-500

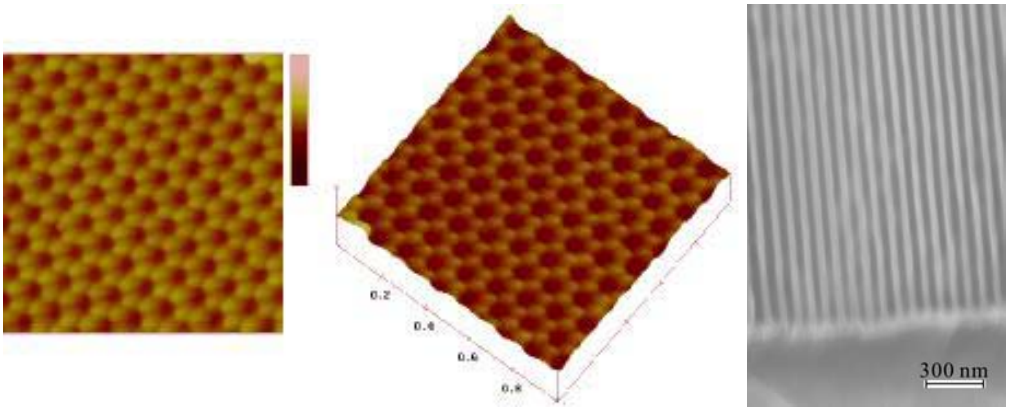

Figure 2. AFM images show topology of the highly ordered alumina pore array and SEM cross-section view of the bottom part of the pore channels (right).

3.1.2. Pore size and inter-pore distance (periodicity) control

As shown in Table 1, we could alter the pore size and inter-pore spacing using different anodization conditions. Our experimental results (as well as other researchers') showed that in a specific solution, both the pore size and the inter-pore spacing, are proportional to the anodization voltage [R6], as shown in Figure 3. Through these correlations, we could easily design our experiments according to the requirements. Figure 4 shows alumina templates with different pore sizes and inter-pore distances by anodizing aluminum in various acid solutions at different voltages. On the other hand, we could also change the pore size via wet etching (pore widening) while keeping the same inter-pore distance as shown in Figure 5.

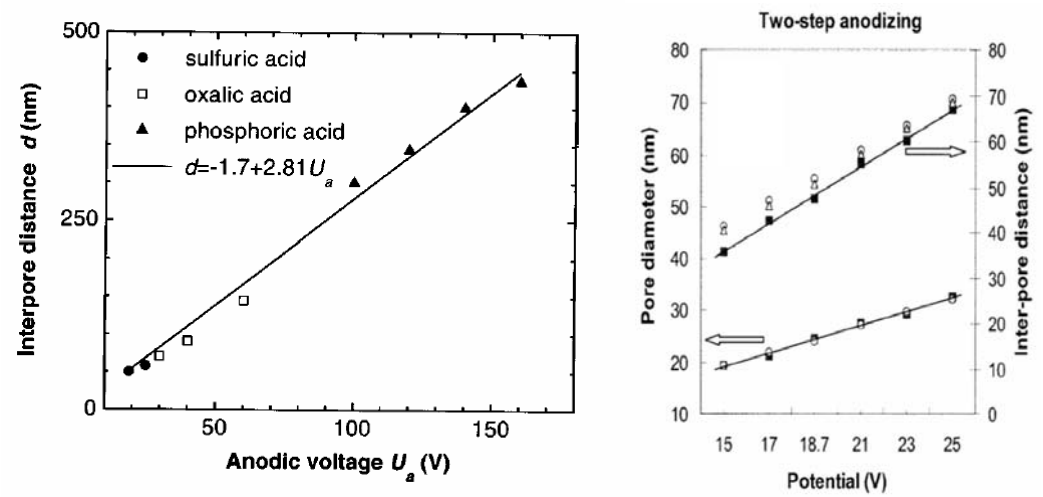

Figure 3. Relationship between pore diameter, inter-pore distance and anodization voltage

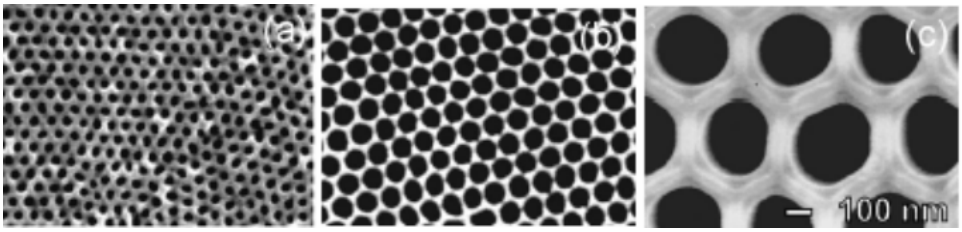

Figure 4. SEM images of alumina pore arrays with different pore diameters and inter-pore distances (a-c: anodized in sulfuric, oxalic, and phosphoric acid at 25, 40, and 196 V, respectively)

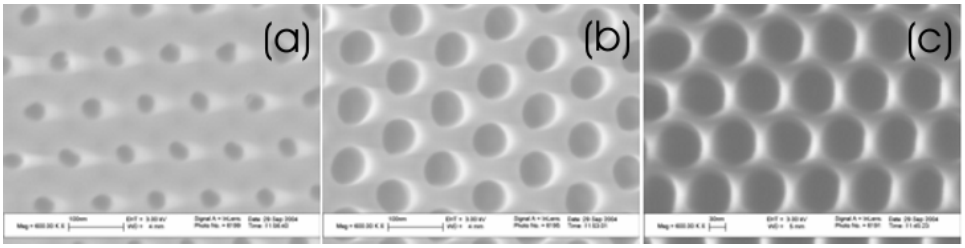

Figure 5. SEM images of alumina pore arrays with the same inter-pore distance but different pore diameters (a-c: anodized in oxalic acid at 40 V and wet-etched in phosphoric acid for 0, 1, and 2 h, respectively)

3.1.3. Thickness control

Under certain conditions, the thickness of the alumina template (d) is proportional to the anodization current density (I) and the anodization time (t). An empirical equation was introduced for precise control of the anodization process based on our results, which can be expressed as:

$$d = C \times I \times t = C \times \frac{i}{A} \times t$$

where i is the anodization current and A is the anodized area of aluminum; C is a constant. In our standard anodization process, i.e., in 0.3 M oxalic acid, at a voltage of 40 V and

temperature of 10 ^{o}C, we obtained that C=0.017 while the units of d, i, A, and t are in μm, mA, cm^2, and min, respectively. This equation was also used for us to estimate the anodization duration if a desired alumina film thickness was specified.

3.1.4. Alumina mask

Three aspects were identified to be very important for preparing the alumina membrane as etching or evaporation mask, which include (1) two-step anodization, as mentioned above; (2) control of the thickness of the alumina membrane during the second anodization; and (3) the wet etching conditions (etchant and time) for removal of the alumina barrier. We are able to controllably fabricate alumina masks with pore diameter and film thickness ranging from 20-80 nm and 200-800 nm, respectively. An alumina mask with pore diameter down to ~10 nm was demonstrated, but the ordering of the pores decreased and precise control was needed. Figure 6 shows an alumina film of highly ordered through-pore array with pore diameter of about 50 nm and film thickness of about 500 nm.

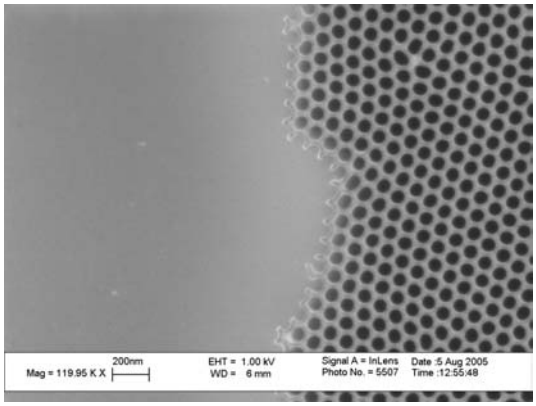

Figure 6. SEM image of a free-standing alumina film/mask on a silicon substrate, viewed along the edge of the alumina film.

3.1.5. Alumina template on other substrates

Since nanostructures (nanowires, nanotubes) grown in freestanding alumina/aluminum templates are limited in applications because they are not readily interfaced electronically with external circuits, it is desirable and often necessary to integrate such nanostructures onto semiconductors (e.g., silicon) such that they can broaden their applications and provide possibilities for incorporating new functionalities with the silicon electronics. To this end, we have extensively investigated the fabrication conditions for obtaining a highly ordered alumina template on silicon substrates [P4], and successfully produced carbon nanotube arrays with unprecedented uniformity directly on silicon, which will be described in detail later (see section 3.3.2).

3.2. Semiconductor highly ordered and densely packed arrays of uniform quantum-dots, quantum-wires, and quantum-heterojunctions

3.2.1. Anti-dot array

Nanopore arrays on various substrates, such as Si, GaN, and GaAs, etc. [R2], were readily fabricated and were further used as second generation templates for other

nanofabrications, e.g., epitaxial growth of quantum dots into the nanopores [R7]. Figure 7 shows nano anti-dot arrays on silicon [P5].

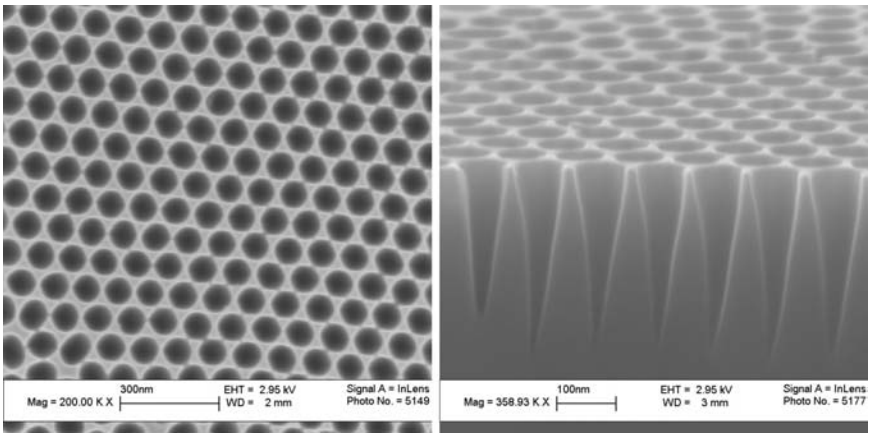

Figure 7. SEM top (left) and cross-sectional (right) view of a nanopatterned silicon substrate

3.2.2. Quantum-wire/nano-pillar array

We also explored the method of making quantum-pillar arrays. The nanostructures were fabricated by etching into existing materials and using an alumina template as an etching mask in the traditional sense. By using a nickel nano-dot array, evaporated through the alumina template, as the RIE etching mask, we successfully fabricated silicon quantum- / nano-pillars (Figure 8a, b). By using an alumina template as mask as well as prolonged RIE etching, we also obtained nano-needle arrays on silicon as shown in Figure 8 (c), (d) [P5].

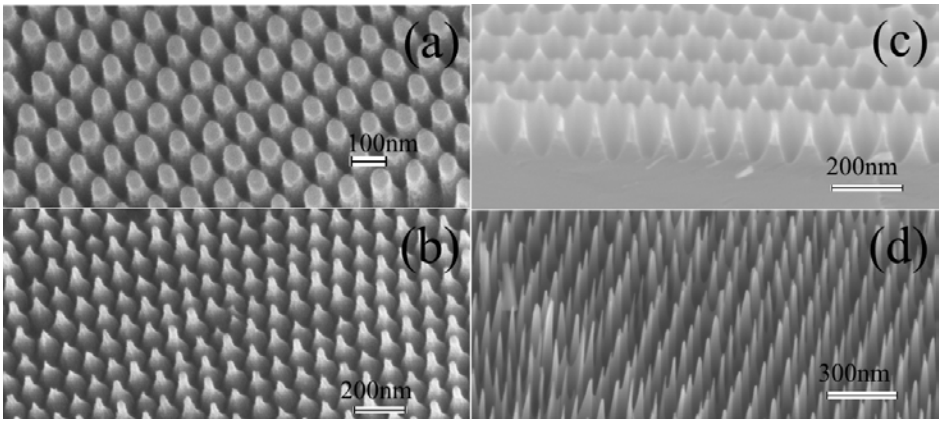

Figure 8. SEM images of Si nanoneedle arrays from using Ni nanodot array as mask (a) and (b) with etching time 5min and 30min, respectively, where the Ni dots were lifted by a Ni etchant after RIE etching; (c) cross-section view of the porous Si from 5min-etch using AAO masks as the short nanopillars emerging around each pore; (d) porous Si with nanoneedles formed at the pore cell corners from 30min-etch using AAO mask.

3.2.3. Quantum-dot (QD) array

The idea to further confine carriers to a greater degree and ultimately reduce the dimensionality to zero, i. e., a quantum dot, has been sought after in the development of electro-

optic devices. When the quantum dots act as the active layer of a semiconductor laser, theoretically the device offers low threshold current density, good temperature characteristics, and broad wavelength tunability. To realize the desired zero-dimensional behavior of a quantum dot ensemble, the ability to fabricate quantum dots with a high packing density and a high degree of size, shape, and spacing uniformity is crucial. Using the same strategy for fabricating nanopillars as described above, a schematic is shown in Figure 9 to illustrate our method for fabricating vertically stacked lateral superlattices of quantum dots. A three-dimensional array of InGaAsN:Sb quantum dots was demonstrated by using this method [R8].

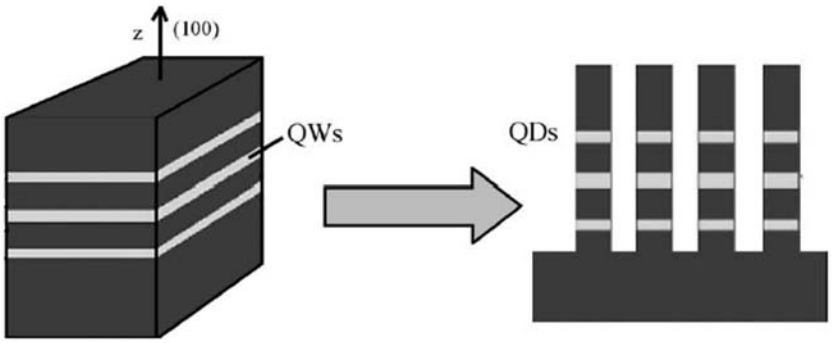

Figure 9. Schematic of transforming an epitaxially grown quantum well structure to a quantum dot structure using an alumina template as a mask

3.3. Organic-inorganic nanocomposite superlattices

3.3.1. Carbon nanotube-alumina composites

Unique structural and electronic properties of carbon nanotubes have been envisioned for prospective applications including field emission displays, biocompatible sensors, and molecular scale electronic and photonic devices to name just a few [R9]. Most of these applications will require a fabrication method capable of producing uniform carbon nanotubes with well-defined and controllable properties. Additionally, the technique employed must be reproducible if any large scale fabrication of carbon nanotubes is envisioned. Efforts to fabricate aligned, isolated carbon nanotubes in an array form have led to considerable and unprecedented success, and arrays of parallel carbon nanotubes with uniform diameters and periodic arrangements have been achieved with the use of the alumina template. The CVD growth of carbon nanotubes using alumina templates was first demonstrated by our group and refined over the years. The highly ordered carbon nanotube arrays (Figure 10) are uniform in length, parallel to each other, and perpendicular to the template [P6].

The highly ordered carbon nanotube arrays have provided not only a good platform for potential large scale nano-electronic applications, but also served as a nanostructured materials base for further development of new structures or devices. For example, we used these carbon nanotube-alumina arrays as a platform for fabrication of carbon nanotube-polymer composites (section 3.3.3.) with potential applications for heat dissipation devices in nano-electronics. We also explored their applications in biosensing by using the carbon nanotube ensemble as nanoelectrode arrays [R10].

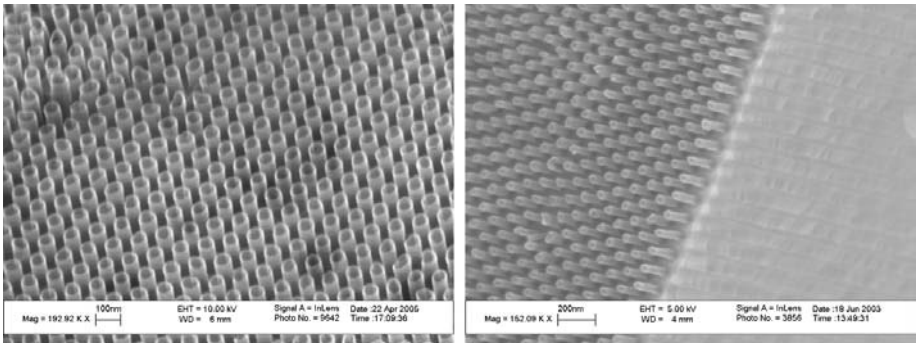

Figure 10. Highly ordered carbon nanotube array in alumina template, with tubes partially exposed by wet etching.

3.3.2. Carbon nanotube-silicon heterojunctions

Using the integrated alumina membrane-silicon as growth template, a highly ordered carbon nanotube array was obtained [P7]. And more importantly, by finely tuning the fabrication conditions, especially of the anodization process, a new type of heterojunction formed between carbon nanotubes and silicon. The pronounced rectifying characteristics of the heterojunction were measured with an on-off ratio as high as 10^5 at 4 V. The analysis showed a large and type-I band offset at the heterojunction. The charge transport in the nanotubes is found to be strongly coupled to and limited by the dielectric charging and polarization in the hosting alumina matrix surrounding the nanotubes [P8, P9] (Figure 11, left).

We also investigate this nanotube-silicon nanostructure with spectral photocurrent measurements in the near and mid-infrared regime in both cooled and uncooled modes of detection. Transient photocurrent analysis suggests that both thermal and direct optoelectronic effects are sources of photoresponse (Figure 11, right). First-principle theoretical treatments of the detection mechanisms imply that performance parameters such as D* could be greatly optimized in future generations of samples. We explore the suitability of this detector prototype for space borne applications where many known properties of carbon such as strong covalent bonding and therefore radiation hardness render it a promising candidate for consideration [P10-P13].

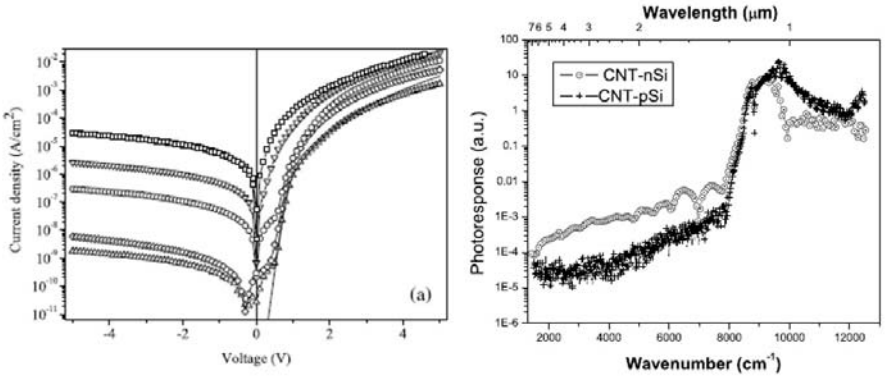

Figure 11. (left) Current voltage characteristics of the CNT-Si structures at different temperatures: squares, 300 K; down triangles, 210 K; circles, 90 K; diamonds, 40 K; and up triangles, 17 K. (right) Photocurrent spectrum of the silicon-nanotube heterojunction with p-type silicon (+) and n-type silicon (o) at room temperature.

3.3.3. Carbon nanotube-polymer composites

Based on analysis and experimental results, CNT-polymer composites can not only be used as a platform for future thermal management and signature reduction, but also as tools for studying the fundamental phase transition in nanoscale. A device of this nature can now be readily manufactured in our lab by a combination of polymer deposition and template-assisted nanotube-array growth methods. A nanotube array hosted in porous anodic alumina could have its template partially removed. The freed ends of the nanotubes can be inserted into a polymer composite (with or without functionalization), followed by the removal of the remaining anodic alumina template. If necessary, the exposed tips of the nanotubes could be functionalized with yet a different material. Figure 12 is an example of integration of AAO-assisted grown CNTs in PDMS matrix. We were able to replace part of the template by PDMS and keep the spacing and also have capabilities to functionalize portion of the CNTs. This would result in a polymer composite heat conductor surface consisting of arrayed nanotube tips, pre-patterned and uniformly structured. The nano-structured surface would provide a facilitated liquid-vapor transition, allowing for the unique size-dependent phenomenon of increase in transition efficiency to occur.

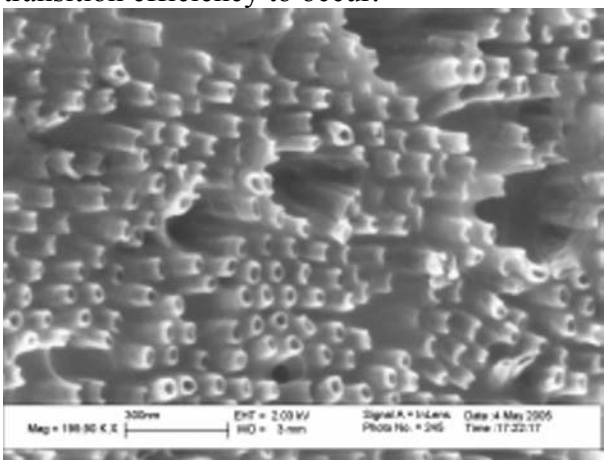

Figure 12. SEM image of carbon nanotube array embedded in polymer (PDMS)

3.3.4. Carbon nanotube-organic nanocomposites

Highly ordered organic–inorganic nanocomposite arrays formed by filling AAO nanopores (50 nm size) with Rhodamine 123 (Rh123) dye have also been studied by visible absorptive, fluorescent spectroscopy, and atomic force/scanning electron microscopy techniques. The absorbance and fluorescence spectra were found to drastically differ from that of conventional Rh123 films deposited onto flat substrates [P14]. The molecular assemblies in the nanopore array are mostly monomer-like, the fluorescence yield is many times higher than the conventional film counterpart and increases after exposure to intense laser illumination, and the fluorescence polarization dependence indicates a preferred molecular orientation along the pore axis. Such nanocomposite arrays open up opportunities in engineering molecular assemblies and in creating functional materials of superior properties for future nanophotonics.

3.3.5. Metal nanotubes and inorganic oxide nanotubes

Using alumina template, various metallic nanotubes, e.g., gold and nickel nanotube arrays, were obtained by electroless deposition. The resultant nanotubes can be served as modification layer to the alumina pores for shrinking the pore size or using as a new platform for nanofabrication. The resultant metal nanotube ensemble, characterized with large surface area, can also be used as nanoelectrode arrays for electrochemical sensing.

On the other hand, through the sol-gel method, we succeeded in fabricating silicon oxide nanotubes or nanowires. The former can also be served as surface modification layer for the alumna nanopores.

3.3.6. Polymer nanotubes /nanowires

By vacuum filling or in situ polymerization, or by electrochemical polymerization/deposition using alumina film as template, polymer nanotube or nanowire arrays can be obtained. For example, we have made PDMS, PMMA, and PPy etc., nano-ensembles in alumna. And recently, much effort has been placed on fabrication of biodegradable polymer nanotubes aimed for drug-delivery and bio-sensing applications.

3.4. Metallic, magnetic, and metal-oxide nanodot and nanowire arrays

3.4.1. Metallic nanodot array

We prepared various metallic nano-dot arrays (Ag, Au, Ni, Co, Fe, etc.) on different substrates (glass, quartz, silicon, GaN, etc.) by using alumina film as evaporation mask in an e-beam evaporator (Figure 13, top). And interesting optical properties were observed. We demonstrated the feasibility of electric-field tuning of the plasmonic spectrum of a novel gold nanodot array in a liquid crystal matrix. As opposed to previously reported microscopically-observed near-field spectral tuning of individual gold nanoparticles, this system exhibited macroscopic far-field spectral tuning. The nanodot-liquid crystal matrix also displayed strong anisotropic absorption characteristics, which can be effectively described as a collective ensemble within a composite matrix in the lateral dimension and a group of noninteracting individual particles in the normal direction (Figure 13, bottom). The effective medium model and the Mie theory were employed to describe the experimental results [P15].

3.4.2. Metal-oxide nanowire/nanorod/nanodot arrays

Through vapor-liquid-solid (VLS) growth method, we successfully fabricated zinc oxide nanoposts on GaN substrates [P2]. Starting with Au nanodots 50 nm in diameter and spaced 110 nm apart center-to-center on the GaN surface after the AAO template has been removed, the patterned GaN substrate was placed onto a ceramic boat downstream from the $ZnAs_2$ source supplying zinc in a horizontal tube furnace. In the sample shown in Figure 14, a growth time of 20 min produced nanorods of 400 nm in average length. The average diameter of the resultant nanorods is 60 nm. The nanorods are vertically aligned with respect to the surface of the GaN and orderly spaced in the hexagonal pattern defined the AAO template deposition of the Au catalysts.

The growth temperature is significantly lower than normal, and yet, the resultant defect level is much lower than normal. Photoluminescence (PL) spectroscopy was performed using an alexandrite laser configured to lase in its third harmonic (252 nm).

Strong exciton emission was observed at room temperature in the ultraviolet region with a peak at 379 nm and a FWHM of 18 nm [P2].

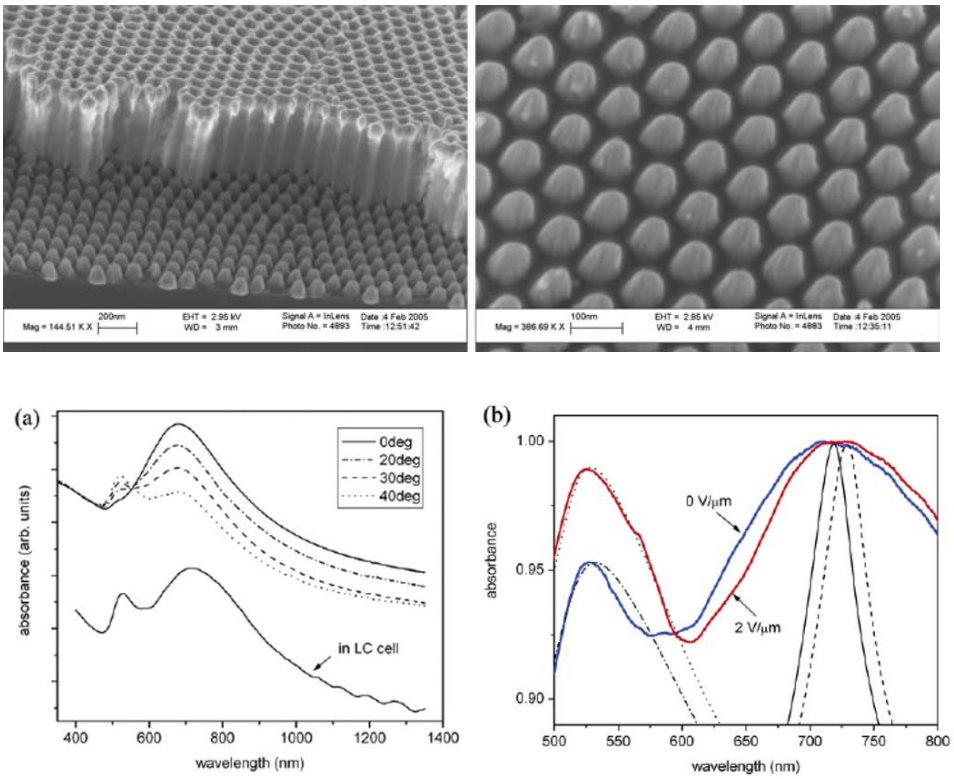

Figure 13. (upper) SEM images of nano-dot array; (bottom) (a) The absorption spectra of an array of gold nanodots on a glass substrate at various angles of light incidence. Normalization of all spectra to unity was performed at the wavelength of 200 nm. The lower spectrum is the absorption of an array of nanodots in a liquid crystal cell under normal incidence of light. (b) The experimental absorption spectra at 0 and 2 V/μm electric fields. The spectra are normalized to unity at the lateral absorption peak wavelength. The fits (field-off and -on states) are shown by the black lines and are based on the effective medium model (solid and dash lines, respectively) and the Mie theory (dash-dot and dot lines, respectively).

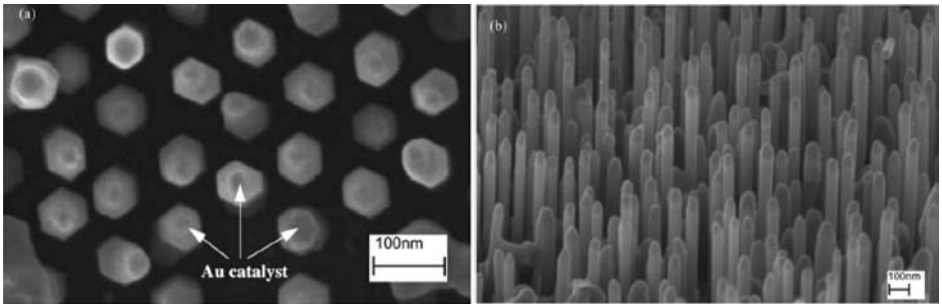

Figure 14. ZnO nanowires grown perpendicularly to the GaN substrate: (a) top view showing hexagonal shaped nanowires with Au catalysts remaining atop and (b) oblique angle view.

3.4.3. Metallic nanowire arrays

Highly ordered hexagonal arrays of parallel metallic nanowires (Ni, Bi) with diameters of about 50 nm and lengths up to 50 um were synthesized by electrodeposition. Hexagonal-close-packed nanochannel anodized aluminum oxide film was used as the deposition template. The deposition was performed in an organic bath of dimethylsulfoxide with metal chloride as the electrolyte. A high degree of ordering and uniformity in these arrays can be obtained with this technique by fine-tuning the electrodeposition parameters. Moreover, an unprecedentedly high level of uniformity and control of the wire length was achieved (Figure 15). The arrays are unique platforms for explorations of collective behavior in coupled mesoscopic systems, and are useful for applications in high-density data storage, field emission displays, and sensors [R5].

Magnetic properties of nano-dot and nanowire arrays were also investigated experimentally and theoretically. Using the same AAO template-assisted nanowire fabrication technique, Nieisch et al. created a similar Ni nanowire array [R11]. Their results showed that each Ni nanowire is expected to be able to be switched independently to the magnetization of its nearest neighbors and thus be able to store 1 bit of information as shown in the magnetic force microscopy image. Theoretical analysis of magnetic properties of the resultant nanodot or nanowire array system was carried out using Monte-Carlo simulation [R12, R13].

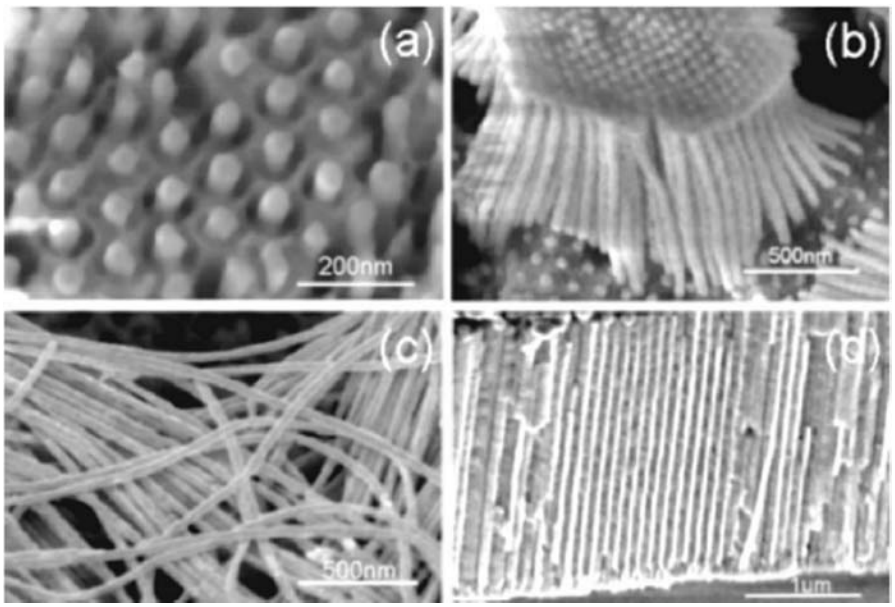

Figure 15. SEM micrographs of nanowire arrays. (a) Top view of Ni nanowire arrays; (b) bundle of Ni nanowires in a 2 μm AAO film after aluminum oxide was partially dissolved; (c) part of the Bi nanowires in a 25 μm AAO template after aluminum oxide was partially dissolved; (d) cross section of the Bi nanowire array, in which the bright lines are Bi nanowires exposed by cracking the template.

3.4.4. Nanostructured Metal Films

Using the alumina films as evaporation substrates, we obtained various nanostructured thin metal films (Figure 16), with potential in magnetic, superconduting, and electrochemical sensing applications [P16].

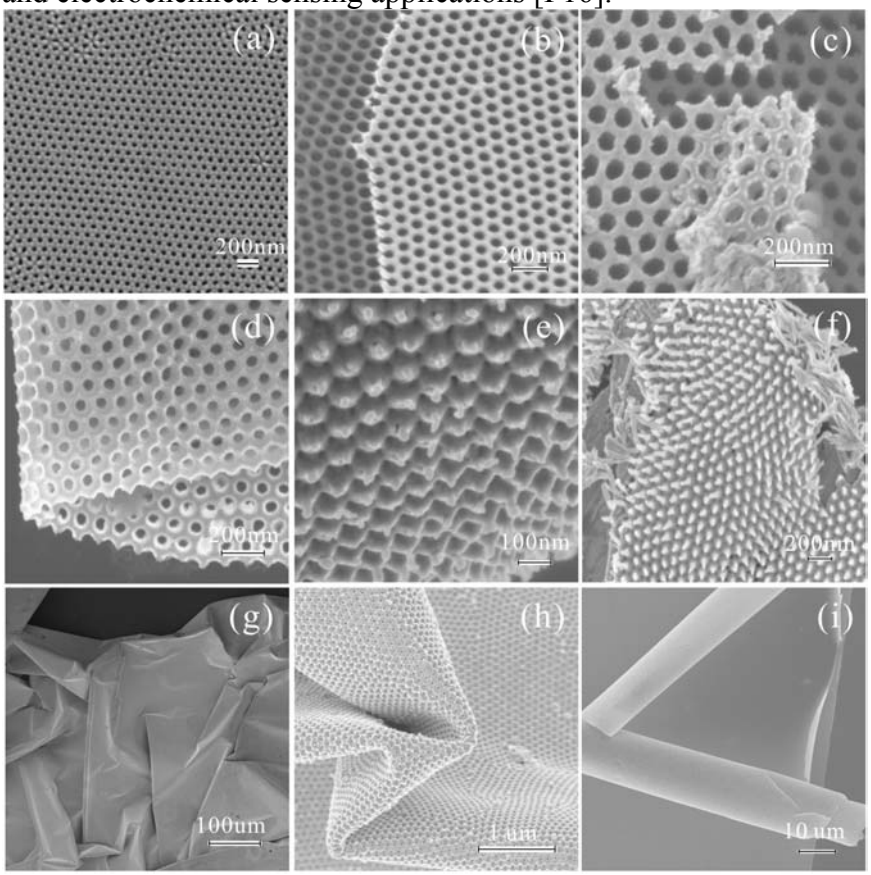

Figure 16. SEM images of the evaporated thin films of various nanostructures: (a)-(c) Porous Ni films before detached from AAO template, where the edge of the metal film on AAO and scratched metal film pieces on AAO were shown in (b) and (c), respectively; (d)-(i) nanostructured films after transferring onto silicon or quartz substrates: (d) porous film; (e) film with nanopore and exposed nanotip array; (f) film with nanotip or nanorod array; (g) stacked or folded film; (h) wrinkle on spread film; and (i) micro film rolls.

We have investigated the structure of films thermally evaporated onto anodic aluminum oxide substrates and revealed mechanism of nanostructure formation. Pb and Sn films spontaneously formed an array of nanometer scale crystals in registry with the holes of AAO substrates. The arrays appeared at film thicknesses at which the metal grain and hole diameters are comparable (Figure 17). Other materials (Au, Pd, Ge) did not form grain arrays. Altogether, our results indicated that arrays form in films that did not wet the substrates and whose grains growed primarily through coalescence. Under these circumstances, the coalescence events were biased by surface energies to drive grains to grow over the holes [P17].

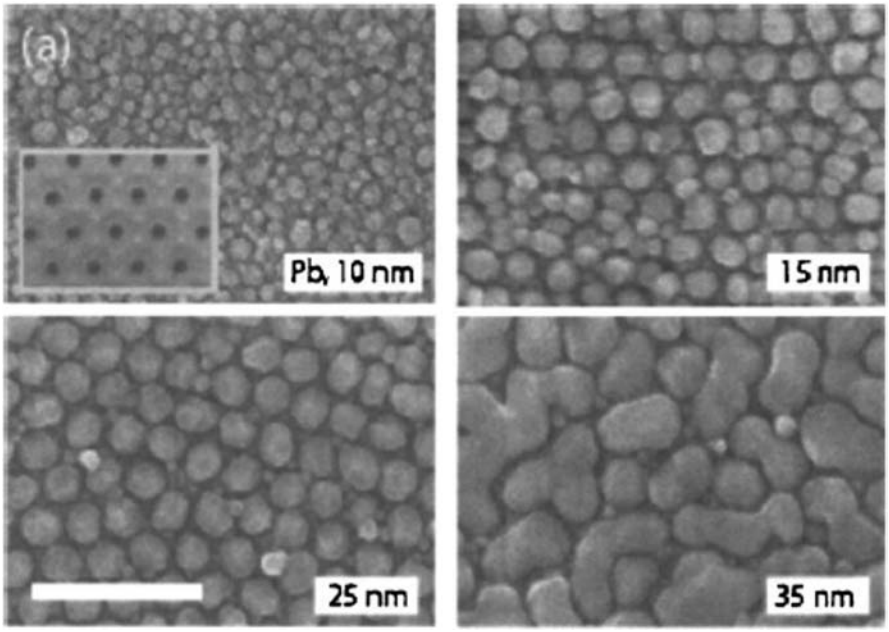

Figure 17. SEM images of Pb films on AAO substrates with 34 nm diameter holes with 100 nm center to center spacing (scale bar: 400 nm). Film thicknesses are indicated in each panel. Inset: Image of a bare substrate.

In the mean time, we have patterned ultrathin Bi/Sb films using alumina template and the magnetic-flux periodic response of the nanoperforated ultrathin superconducting films was investigated. These regular perforations resulted in a phase-sensitive periodic response to an applied magnetic field. Thus by measuring this response in the resistive transitions, we were able to distinguish between superconducting fluctuations of the amplitude and phase. Our results delineated three distinct portions of the *R(T)* in which fluctuations of the amplitude, both the amplitude and phase, and the phase of the superconducting order parameter dominated. In addition, as Tc_0 was lowered, the region of the superconducting transition dominated by amplitude fluctuations was large and grew with proximity to the superconductor to insulator transition [P18, P19].

4. CONCLUSIONS

A non-lithographic nanofabrication method was devised, developed and optimized for fabrication of nanometric superlattices aimed for radiation and magnetic sensing. Central to the non-lithographic nanofabrication method was the utilization of an alumina nanopore membrane as either the growth template, or etch or evaporation mask for the formation of the proposed nanostructures. In the past few years, we explored all the research aspects with devotion, effort, and all the means available to us, and delivered various kinds of nanometric superlattices, as proposed and stated in the program. These include:

(1) We further optimized the aluminum anodization process for obtaining a highly ordered porous alumina template. The most important progress/achievements include (a) We created a wet-solution process for obtaining a highly ordered porous alumna mask, which served as the center piece for most of the nanopatterning fabrications; (b) We extensively investigated the process for integrating an alumina film onto a silicon substrate. By

having a custom-designed new E-beam evaporation system, we were able to obtain high-quality aluminum films with unprecedented thickness (over 40 μm) and therefore to grow highly-ordered AAO templates or CNT arrays directly on silicon substrates.

(2) In the first thrust for fabrication of semiconductor highly-ordered and densely-packed arrays of uniform quantum-dots, quantum-wires, and quantum heterojunctions, we were able to obtain various nanostructured materials, including anti-dot arrays on SOI, GaN, and GaAs substrates. The optical properties of the nanostructures were also studied.

(3) In the second thrust for organic-inorganic nanocomposite superlattices, we provided and studied a series of carbon nanotube (CNT) -inorganic/organic nanocomposite materials, including CNT-alumina composite, CNT-Si heterojunctions, CNT-PDMS composite, CNT-DNA composite, and CNT-ZnO structures. We also investigated some metal or oxide nanotube/nanowires, such as, Ni, Au, and SiO_2. In addition, we studied dye and liquid crystal filled alumina composites as well as polymer nanotubes/nanowires.

(4) In the third thrust for metallic, magnetic, and metal-oxide nanodot and nanowire arrays, we were able to fabricate nanodot arrays of Ag, Au, Ni, Co, Fe, Nb, etc. on various substrates; We have made metal oxide nanowire arrays (ZnO nanowires on GaN substrate) and metallic nanowire arrays (e.g., Ni, Bi).

(5) More than proposed, we fabricated and investigated some other interesting nanostructures, such as nanostructured thin films (Au, Ag, Ni, Nb, Bi, Pb, etc.), polymer nanotubes, etc., which are productions extended or derived from the work supported by this program.

(6) We have published 21 peer-reviewed papers on the above mentioned fronts in several renowned journals including Physics Review Letters, Applied Physics Letters, and so on. We also had numerous presentations in professional conferences or invited talks.

5. PUBLICATIONS

[P1] a) H. Chik, and J. M. Xu, "*Nanometric superlattices: non-lithographic fabrication, materilas, and prospects*", Mater. Sci. Eng. R43, 103, 2004; b) T. F. Kuo, and Jimmy Xu, "*Growth and application of highly ordered array of vertical nanoposts*", J. Vac. Sci. Technol. B24, 1925, 2006

[P2] H. Chik, J. Liang, S. G. Cloutier, N. Kouklin, and J. M. Xu, "*Periodic array of uniform ZnO nanorods by second-order self-assembly*", Appl. Phys. Lett. 84, 3376, 2004

[P3] Aijun Yin, Rodney Guico, and Jimmy Xu, "*Fabrication of Anodic Aluminum Oxide Templates on Curved Surfaces*", Nanotechnology, 18, 035304, 2007

[P4] A. J. Yin, M. Tzolov, D. Cardimona, L. Guo, and J. M. Xu, "*Fabrication of highly ordered anodic aluminum oxide template on silicon substrate*", IET, Circuits, Devices & Systems, 2007, in press.

[P5] Aijun Yin and Jimmy Xu, "*Fabrication of Highly-ordered and Densely-packed Silicon Nano -needle Arrays for Bio-sensing Applications*", Mater. Res. Soc. Symp. Proc. Vol. 900E, 2006 Materials Research Society 0900-O11-02.1

[P6] Aijun Yin, Hope Chik, and Jimmy Xu, "*Post-growth processing of carbon nanotube arrays - Enabling new functionalities and applications*", IEEE Trans. Nanotech. 3(1), 147, 2004

[P7] Aijun Yin, Marian Tzolov, David Cardimona and Jimmy Xu, "*Template-Growth of Highly Ordered Carbon Nanotube Arrays on Silicon*", IEEE Transactions on Nanotechnology, 5, 564-567, 2006

[P8] M. Tzolov, B. Chang, A. Yin, D. Straus, and J. M. Xu, *"Electronic transport in controllably grown carbon nanotube-silicon heterojunction array",* Phys. Rev. Lett. 92(7), 075505-1, 2004

[P9] a) Marian B. Tzolov, Baohe Chang, Daniel Straus, Aijun Yin, and Jimmy Xu, "*Carbon Nanotube-Silicon Heterojunction Diode Array – Integration on Silicon and Rectifying Characteristics*", MRS Proc., M8.22, 2004; b) T. F. Kuo, and Jimmy Xu, "*Growth of vertical and highly ordered carbon nanotube – silicon heterojunction diode array*", MRS, Proc. Vol.901E, 0901-R005-17-Rb05-17.1, 2006

[P10] M. B. Tzolov, T. F. Kuo, D. A. Straus, A. J. Yin, amd J. M. Xu, "*Carbon nanotube-silicon heterojunction arrays and infrared photocurrent responses*", J. Phys. Chem., C111, 5800, 2007

[P11] D. A. Straus, M. Tzolov, A. J. Yin, T. F. Kuo, S. G. Cloutier, and J. M. Xu, "*Hybrid nanostructures for mid-infrared detection*", Proc. SPIE Int. Soc. Opt. Eng. 5897, 58970O, 2005

[P12] M. B. Tzolov, D. Straus, A. J. Yin, and J. M. Xu, "*Arrayed carbon nanotube infrared properties and potential applications*", Proc. SPIE Int. Soc. Opt. Eng. 5543, 56, 2004

[P13] D. Straus, M. Tzolov, T. F. Kuo, A. J. Yin, and J. M. Xu, "*Photocurrent response of the carbon nanotube-silicon heterojunction array*", IET, Circuits, Devices & Systems, 2007, in press

[P14] I. A. Levitsky, J. Liang, and J. M. Xu, "*Highly ordered arrays of organic–inorganic nanophotonic composites*", Appl. Phys. Lett. 81, 1696, 2002

[P15] Pavel. A. Kossyrev, Aijun Yin, Sylvain G. Cloutier, David A. Cardimona, Danhong Huang, Paul M. Alsing, and Jimmy M. Xu , *"Electric Field Tuning of Plasmonic Response of Nanodot Array in Liquid Crystal Matrix",* Nano Lett., 5(10), 1978-1981, 2005

[P16] A. J. Yin, J. Kim, and Jimmy Xu, "*Templated fabrication of nanostructured thin films*", MRS Proc. Vol.951, 0951-E09-15, 2006

[P17] N. Pavenayotin, M. D. Stewart, Jr., J. M. Valles, Jr., A. J. Yin, J. M. Xu, *"Spontaneous formation of Ordered Nanocrystal Arrays in films Evaporated onto Nanopore Array Substrates"*, Appl. Phys. Lett., 87, 193111, 2005

[P18] M. D. Stewart, Jr., Zhenyi Long, J. M. Valles, Jr., Aijun Yin, and J. M. Xu, "*Magnetic-flux periodic response of nanoperforated ultrathin superconducting films*", Phys. Rev. B 73, 092509, 2006

[P19] M. D. Stewart, Jr., Aijun Yin, J. M. Xu, and James M. Valles, Jr., "*Superconducting pair correlations in an insulating nano-honeycomb film*", submitted to Nature.

6. REFERENCES

[R1] J. Liang, H. Chik, A. Yin, and J. M. Xu, "*Two-dimensional lateral superlattices of nanostructures: Nonlithographic formation by anodic membrane template*", J. Appl. Phys. 91, 2544, 2002

[R2] J. Liang, H. Chik, and J. M. Xu, "*Nano-lithographic fabrication of lateral superlattices for nanometric electromagnetic-optic applications*", IEEE Journal of Selected Topics in Quantum Electronics, 8, 998, 2002

[R3] H. Masuda and K. Fukuda, Science 268, 1466, 1995

[R4] J. Li, C. Papadopoulos, J. M. Xu, and M. Moskovits, "*Highly-ordered carbon nanotube arrays for electronics applications*", Appl. Phys. Lett. 75, 367, 1999
[R5] A. J. Yin, J. Li, W. Jian, A. J. Bennett, and J. M. Xu , "*Fabrication of highly ordered metallic nanowire arrays by electrodeposition",* Applied Physics Letters Vol 79(7) pp. 1039-1041. August 13, 2001
[R6] A. P. Li, F. Mu¨ ller, A. Birner, K. Nielsch, and U. Go¨sele, "*Hexagonal pore arrays with a 50–420 nm interpore distance formed by self-organization in anodic alumina*", J. Appl. Phys. 84, 6023, 1998
[R7] J. Liang, H. Luo, R. Beresford, and Jimmy Xu, "*A growth pathway for highly ordered quantum dot arrays*", Appl. Phys. Lett. 85, 5974, 2004
[R8] N. Kouklin, H. Chik, J. Liang, M. Tzolov, J. M. Xu, J. B. Heroux, and W. I. Wang, "*Highly periodic, three-dimensionally arranged InGaAsN:Sb quantum dot arrays fabricated nonlithographically for optical devices*", J. Phys. D 36, 2634, 2003
[R9] Jimmy Xu, "*Nnaotube Electronics: Non-CMOS routes*", Proc. IEEE 91, 1819, 2003
[R10] G. D. Withey, A. D. Lazareck, M. B. Tzolov, A. Yin, P. Aich, J. I. Yeh, and J. M. Xu, "*Ultra-high redox enzyme signal transduction using highly ordered carbon nanotube array electrodes*", Biosensors and Bioelectronics, 21, 1560-1565, 2006
[R11] K. Nieisch, R.B. Wehrspohn, J. Barthel, J. Kirschner, U. Gosele, S.F. Fischer, H. Kronmuller, Appl. Phys. Lett. 79, 1360, 2001
[R12] A. J. Bennett and J. M. Xu, "*Simulating collective magnetic dynamics in nanodisk arrays*", Appl. Phys. Lett. 82, 2503, 2003
[R13] A. J. Bennett and J. M. Xu, "*Simulating the magnetic susceptibility of magnetic nanowire arrays*", Appl. Phys. Lett. 82, 3304, 2003

7. ATTACHMENT: GLOSSARY OF ABBREVIATIONS AND ACRONYMS

Abbreviations and Acronyms	***Definitions***
2D, 3D	Two-dimensional, three-dimensional
AAO	Anodic aluminum oxide
AFM	Atomic force microscope
AFRL	Air Force Research Laboratory
CNT	Carbon nanotube
CVD	Chemical vapor deposition
DNA	Deoxyribonucleic acid
DoD	Department of Defense
E-beam	Electron beam
EDX	Energy dispersive X-ray
FTIR	Fourier transfer infrared
FWHM	Full width at half maximum
HRTEM	High-resolution transmission electron microscope
MBE	Molecular beam eptitaxial
MFM	Magnetic force microscope
PDMS	Polydimethylsiloxane
PL	Photoluminescence
PMMA	Poly(methyl methacrylate)
PPy	Polypyrrole
QD	Quantum dot
QW	Quantum well
Rh123	Rhodamine 123
RIE	Reactive ion etching
SEM	Scanning electron microscope
SOI	Silicon on insulator
TEM	Transmission electron microscope
VLS	Vapor-liquid-solid
XRD	X-ray diffrarction

DISTRIBUTION LIST

DTIC/OCP
8725 John J. Kingman Rd, Suite 0944
Ft Belvoir, VA 22060-6218 1 cy

AFRL/VSIL
Kirtland AFB, NM 87117-5776 2 cys

AFRL/VSIH
Kirtland AFB, NM 87117-5776 1 cy

Official Record Copy
AFRL/VSSS, Dr. DanHong Huang 1 cy